Magnetically Tunable Graphene-Based Terahertz Metasurface

Yafeng Lu[1,2], Chen Wang[1], Shiqiang Zhao[1] and Yongzheng Wen[1]*

[1]State Key Laboratory of New Ceramics and Fine Processing, School of Materials Science and Engineering, Tsinghua University, Beijing, China, [2]Army Aviation Institute of PLA, Beijing, China

Graphene is a promising platform for configurable terahertz (THz) devices due to its reconfigurability, but most researches focus on its electrical tunability. Here, we propose a graphene-based THz metasurface comprised of graphene cut-wire arrays for magnetic manipulation of the THz wave. With the external magnetostatic field applied, the resonant currents of the graphene cut-wire can be effectively affected by the Lorentz force, leading to an evident tuning of the response of the metasurface. The simulated results fully demonstrate that the resonance frequencies of the graphene THz metasurface can be efficiently modulated under a vertical magnetostatic field bias, resulting in the manipulation of the transmittance and phase of the THz wave. As a new method of the tunable THz metasurface, our structure shows promising applications in the THz regime, including the ultracompact THz modulators and magnetic field sensors.

Keywords: graphene, magnetostatic field, dynamically tunable, terahertz metasurface, Lorentz force

INTRODUCTION

The terahertz (THz) band lies in the frequency gap between the infrared and microwaves and possesses the characteristics of both photonics and electronics [1], making the THz wave of great perspective in material characterization [2], biomedical sciences [3], and wireless communication [4–7]. In the development of THz technology, effective manipulation of THz waves is particularly important, which still remains challenging in practical application. The emergence of metamaterial provides an approach to surmount this dilemma. Metamaterials are composed of periodic or aperiodic subwavelength scale artificial unit structures, exhibiting extraordinary electromagnetic properties [8–12]. The electromagnetic response of the incident waves can be flexibly customized to satisfy the application needs [13]. As a two-dimensional metamaterial, metasurfaces have been widely applied in THz modulators, switchers, phase shifters, and sensors [14–17] due to their advantages of ultrathin and easy to implement.

Early studies on the THz metasurface mainly rely on changing the structural parameters to meet the required electromagnetic characteristics. Although excellent functions can be achieved, once the devices are prepared, their electromagnetic response characteristics are fixed and cannot be tuned, which limits the practical applications of metasurfaces. The tunable THz metasurface can simplify device design [17], and can effectively reduce cost [17], and make it multifunctional. On the other hand, graphene has the intriguing properties of high mobility, strong light-matter interaction, and excellent chemical stability [18]. Although there are still many challenges, graphene with ultra-high mobility and ultra-thin thickness may produce transistors with higher speed and shorter channel length [19], which might have the potential to replace conventional silicon-based semiconductors as the next generation of mainstream semiconductor materials. Some recent work has demonstrated

FIGURE 1 | (A) Schematic diagram of the proposed terahertz metasurface consisting of periodically arranged graphene cut-wire resonators. The structural parameters: $P_x = 250$ μm, $P_y = 500$ μm, $l = 450$ μm, $w = 210$ μm, and the SiO$_2$ substrate has thickness $h = 50$ μm. Conceptual schematic diagram of the oscillation of the electrons in the unit cell (B) without or (C) with the external magnetostatic field applied. When the magnetostatic field bias is applied, the electron oscillation path along the y-axis in the unit cell is deflected at a certain angle.

that graphene can be utilized to realize tunable THz metasurface by changing the Fermi level by electrical bias [20–24]. Besides that, the unique responses of graphene to the light, heat, and force also allow one to actively tune the metasurface with various physical fields [23, 25, 26]. Using this feature, many active tunable graphene devices with excellent performance have been designed and verified by simulation [27–29] or/and experiments [30, 31]. These results indicate that the graphene platform can play an important role in the design of actively tunable THz metasurfaces. Among them, however, the modulation characteristics of the graphene metasurface by the magnetostatic field seems less investigated. It is a well-known fact that when a magnetostatic field is applied in the vertical direction of a two-dimensional conductor, the carrier's motion in which will be deflected due to the Lorentz force [32]. We postulate that when the magnetostatic field is applied perpendicularly to a patterned graphene metasurface, the resonance properties of which under the irradiation of THz waves would be apparently modulated due to the deflection of the direction of the carrier's oscillation in graphene.

In this work, we suggest a magneto-controlled method to manipulate the transmittance properties of the incident THz wave, and proposed a graphene-based THz metasurface comprised of graphene cut-wire arrays for proof-of-principle demonstration. By applying different values of magnetic flux density, the transmittance related parameters of the proposed metasurface can be dynamically controlled. We show that the transmittance properties of graphene THz metasurface can be dynamically controlled by applying an external magnetostatic field perpendicular to the metasurface.

STRUCTURE DESIGN AND PHYSICAL MECHANISM

Figure 1A shows the schematic diagram of the proposed tunable graphene metasurface on top of a SiO$_2$ substrate. The graphene pattern, cut-wire resonators, are periodically arranged in the x–y plane and the structural parameters are denoted. The proposed graphene metasurface is excited by the electric field of a normally incident THz plane wave propagating in the z-axis direction.

When electromagnetic waves irradiate perpendicularly to planar graphene, plasmonic oscillation will occur on the surface of the graphene, and the direction of carrier oscillation is along the electric field, as shown in **Figure 1B**. In this case, if the magnetostatic field is applied vertically to the planar graphene, the oscillation direction of the carriers will no longer follow the direction of the electric field and would be deflected at a certain angle, as shown in **Figure 1C**. The angle is related to the value of the applied magnetic flux density. If the graphene layer is patterned, different angle corresponds to different oscillation environments, the changes of carriers' oscillation will lead to the changes of transmittance properties and result in the resonance frequency shifts and the transmittance shifts.
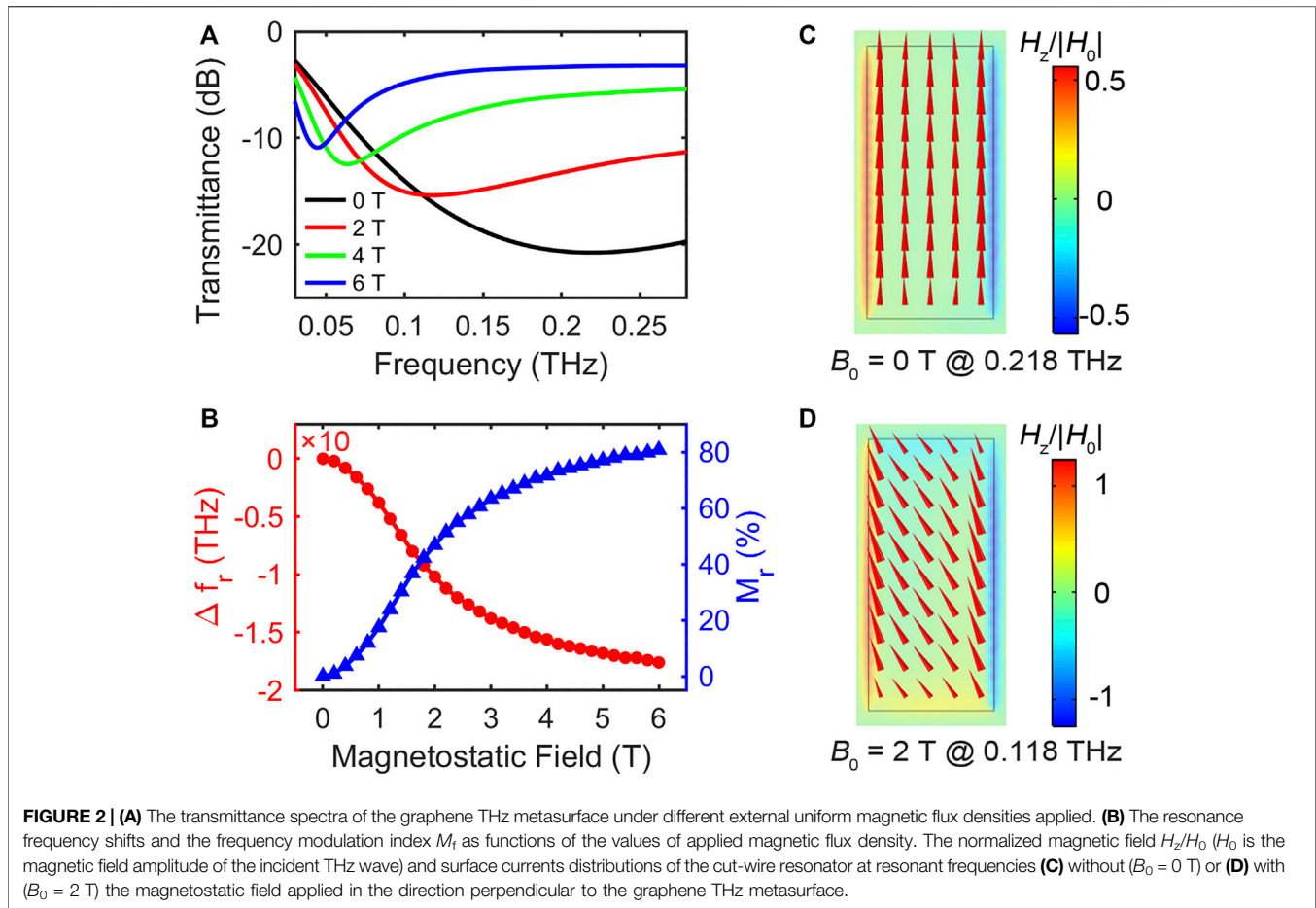
As a two-dimensional (2D) material, graphene can be described by surface conductivity. In our case, the photonic energy of the terahertz frequency is far below the double Fermi level of graphene, and only the intra-band conductivity of graphene is considered, which can be described as [33]:

$$\sigma_s(\omega) = \frac{i \cdot e^2 k_B T}{\pi \hbar^2 (\omega + i\tau^{-1})} \ln\left[2\cosh\left(\frac{E_F}{2k_B T}\right) \right], \quad (1)$$

where e is the electron charge, k_B is the Boltzmann's constant, T is the environmental temperature, $\hbar$ is the reduced Planck's constant, and ω is the angular frequency of incident THz, τ is the relaxation time, E_F is the Fermi energy away from the Dirac point. To achieve the evident resonance of the metamaterial, the Fermi level of the graphene should satisfy $E_F \gg k_B T$, the graphene surface conductivity is further simplified to

$$\sigma_s(\omega) = \frac{i \cdot e^2 E_F}{\pi \hbar^2 (\omega + i\tau^{-1})}, \quad (2)$$

As we referred previously, when the magnetostatic field is applied in the direction perpendicular to the planar graphene, the oscillation direction of the carriers will be deflected. In our proposed configuration, the carriers' motion would be

FIGURE 2 | **(A)** The transmittance spectra of the graphene THz metasurface under different external uniform magnetic flux densities applied. **(B)** The resonance frequency shifts and the frequency modulation index M_f as functions of the values of applied magnetic flux density. The normalized magnetic field H_z/H_0 (H_0 is the magnetic field amplitude of the incident THz wave) and surface currents distributions of the cut-wire resonator at resonant frequencies **(C)** without ($B_0 = 0$ T) or **(D)** with ($B_0 = 2$ T) the magnetostatic field applied in the direction perpendicular to the graphene THz metasurface.

deflected by the Lorentz force. Accordingly, the graphene surface conductivity should include the presence of the magnetic field. Then, in the configuration of **Figures 1A,C**, the new graphene surface conductivity can be described by an anisotropic conductivity tensor [32, 34]:

$$
\overset{\leftrightarrow}{\sigma}_s(\omega) = \sigma_s(\omega)
\begin{bmatrix}
\dfrac{1}{1 + (\mu_e B)^2} & -\dfrac{\mu_e B}{1 + (\mu_e B)^2} & 0 \\[2ex]
\dfrac{\mu_e B}{1 + (\mu_e B)^2} & \dfrac{1}{1 + (\mu_e B)^2} & 0 \\[2ex]
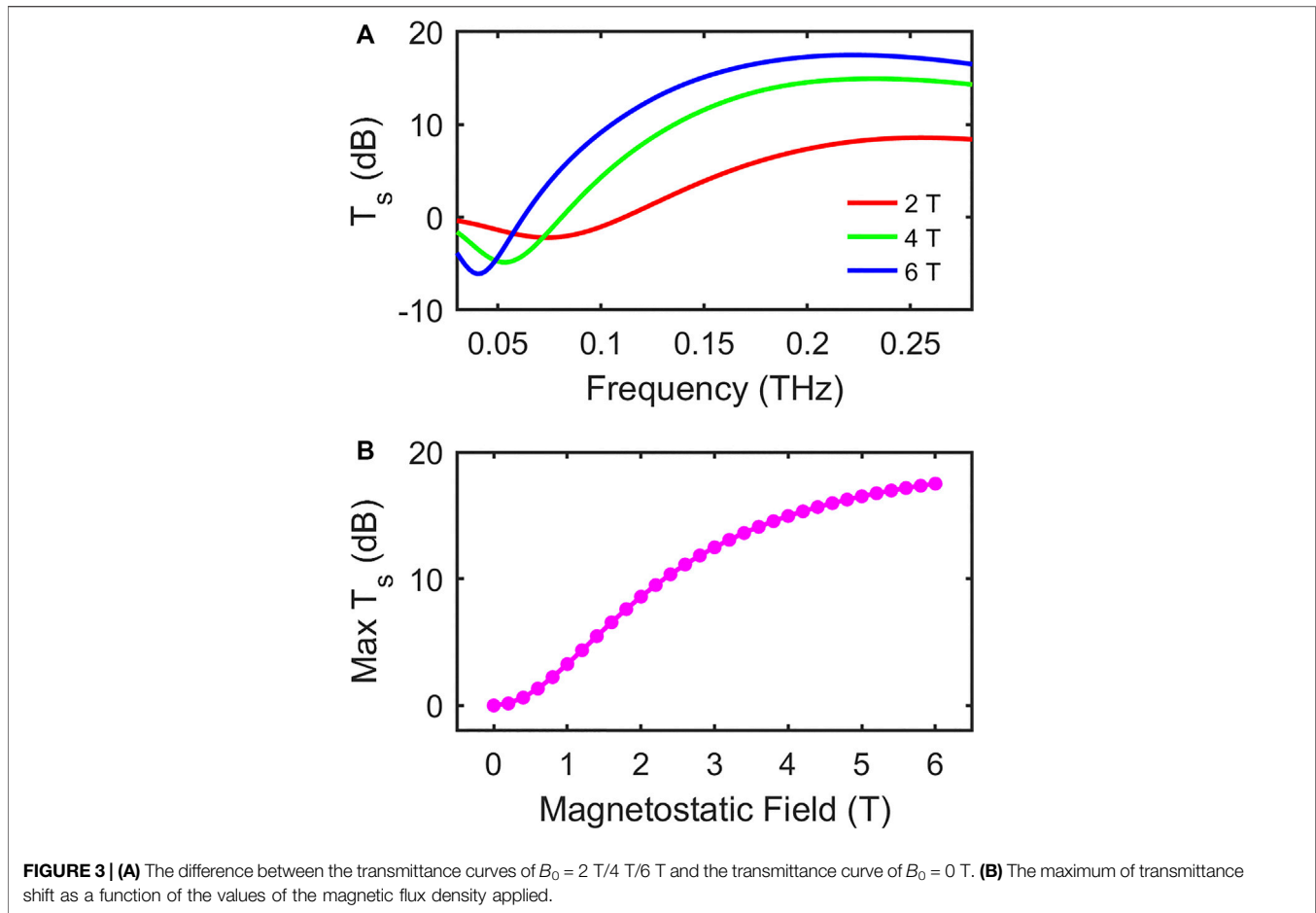0 & 0 & 1
\end{bmatrix}, \quad (3)
$$

where $\sigma = \sigma_0/(1 - i\omega\tau^{-1})$. and $\mu_e = \mu_{e0}/(1 - i\omega\tau^{-1})$. are the optical conductivity and mobility at frequency ω, respectively. σ_0 and μ_{e0} are dc conductivity and mobility, respectively.

The modeling and simulation of the designed terahertz tunable graphene metasurface were performed by COMSOL Multiphysics package, using a lossless dielectric constant $\varepsilon = 3.5$ for the SiO_2 substrate and Fermi level $E_F = 0.35$ eV for the graphene. The complex surface conductivity of the graphene patterns in the model is calculated by the anisotropic conductivity tensor described in **Eq. 3**. Periodic boundary conditions are used in the x-y plane and the y-polarized terahertz wave is normally incident from the top. The

magnetostatics fields are set along the z-axis. In this scheme, although all graphene patches are separated from each other, it is still feasible to control the Fermi level of the whole graphene metasurface in practice. Possible approaches include electrostatic bias and chemical doping. For electrostatic bias, a sandwich structure of ion gel/graphene patterns/ITO configuration [35] could be designed and the electrical bias could be applied at both ends to achieve the modulation of Fermi level. For chemical doping, the graphene patterns could be exposed to nitric acid vapor or nitrogen dioxide [36]. By adjusting the doping and baking time to obtain different doping concentrations, the desired Fermi level could be obtained.

RESULTS AND DISCUSSIONS

We calculated the transmittance spectra of patterned graphene metasurface on SiO_2 substrates with different uniform magnetic flux densities. The wave vector of the planar THz wave is parallel to the z-axis and the electric field is along the y-axis. **Figure 2A** shows the transmittance spectra of the patterned graphene THz metasurface under different external uniform magnetic flux densities applied. It is found that there is an evident resonance dip existing around 0.218 THz without the external

FIGURE 3 | (A) The difference between the transmittance curves of B_0 = 2 T/4 T/6 T and the transmittance curve of B_0 = 0 T. **(B)** The maximum of transmittance shift as a function of the values of the magnetic flux density applied.

magnetostatic field applied (the value of the applied magnetic flux density is 0, black curve). The resonance dip of the metasurface redshifts continuously from 0.218 to 0.044 THz with the increase of the values of magnetic flux density of the applied magnetostatic field from 0 to 6 T, as shown in **Figure 2A**. The resonance frequency shift (Δf_r), defined as the offset between the resonance frequencies with and without the external magnetostatic field is applied, as a function of the values of the applied magnetic flux density is revealed in **Figure 2B**. The effect of frequency modulation is mainly represented by the frequency modulation index [37], here we show the connection of the frequency modulation index and the applied external magnetostatic field. The frequency modulation index was defined as the ratio of the maximum frequency absolute deviation to the operating frequency
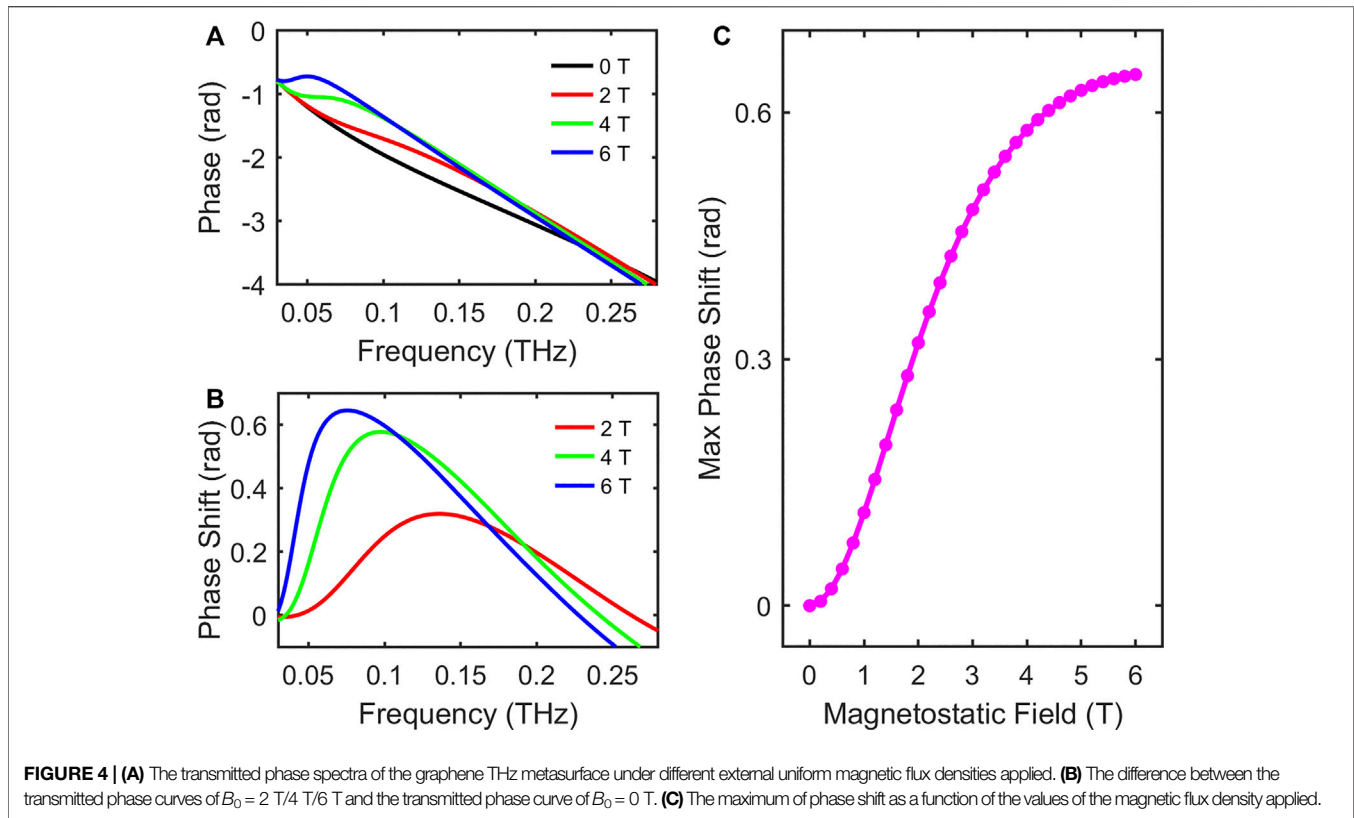
$$M_f = \frac{|\Delta f_r|}{f_0} \times 100\%, \qquad (4)$$

where f_0 is the resonance frequency when the external magnetostatics field is not applied, and Δf_r is the resonance frequency shift induced by the applied external magnetostatics field. The frequency modulation index M_f is also a function of the values of the applied magnetic flux density, as shown in **Figure 2B**. To accurately understand the physical principles

behind this phenomenon, we study the magnetic field H_z and surface currents distributions of the cut-wire resonator at resonant frequencies under corresponding magnetostatic fields. **Figures 2C,D** give the field distributions at 0.218 THz under 0 T magnetic flux density and at 0.118 THz under 2 T magnetic flux density, respectively.

The resonance that occurred at 0.218 THz is obvious a fundamental electric dipolar mode [28], in which the surface currents oscillate straightly along the axial direction driven by the electric field of the incident THz wave, as shown in **Figure 2C**. The introduction of the magnetic field provides the transverse component of the currents and causes the apparent currents deflection due to the Lorentz force on the charge carriers in the graphene cut-wire resonator, **Figure 2D**. Due to the restriction from the pattern, the change of carrier oscillation direction would lead to the change of the field distribution in the cut-wire resonator, resulting in the shift of the resonance frequency. Therefore, the resonance frequency shift in **Figure 2B** and the simulated field distribution at the resonance frequency given in **Figure 3D** well supported our hypothesis.

To now, we have clarified the physics of the metasurface proposed and directly given the numerical proof of carrier deflection under the bias of the external magnetostatic field. The frequency shifts and the changes of the field distribution show that we can control the resonance frequency of the patterned metasurface

FIGURE 4 | (A) The transmitted phase spectra of the graphene THz metasurface under different external uniform magnetic flux densities applied. **(B)** The difference between the transmitted phase curves of $B_0 = 2$ T/4 T/6 T and the transmitted phase curve of $B_0 = 0$ T. **(C)** The maximum of phase shift as a function of the values of the magnetic flux density applied.

through an external magnetostatic field. By introducing different values of the magnetic flux density, dynamic control of the resonance characteristics of the metasurface is achieved.

Besides the resonance frequency shifts, we also investigated the transmittance and the transmitted phase characteristics of graphene THz metasurface. It is found that the transmittance changes significantly when different magnetostatic fields are applied, and the transmitted phase was sensitive to the external magnetostatic field. The change in the transmittance shift was defined as [38].

$$T_s \text{ (dB)} = T_{on} \text{ (dB)} - T_{off} \text{ (dB)}, \quad (5)$$

where T_{on} (dB) is the transmittance of the graphene metasurface when a magnetostatic field is applied; T_{off} (dB) is the transmittance of the graphene metasurface without magnetostatic field (or $B_0 = 0$ T) applied. Taking the transmittance curve of $B_0 = 0$ T (black curve in **Figure 2A**) as a reference, the difference between the transmittance curve of $B_0 = 2$ T/4 T/6T and the transmittance curves of $B_0 = 0$ T are shown in **Figure 3A**. It can be seen easily in **Figure 3B** that the maximum values of the transmittance shifts increase with the increase of applied flux density.

Figure 4A plots the transmitted phase spectra for different values of magnetic flux density applied. It is shown that the transmitted phase response of the metasurface varies greatly under different magnetostatic fields applied. Additionally, we notice that the increase in the values of magnetic flux density applied leads to a clear increase variation of the transmitted phase. To better analyze the variation of transmitted phases, we

take the transmitted phase curve of $B_0 = 0$ T (black curve in **Figure 4A**) as a reference, the difference between the transmitted phase curves of $B_0 = 2$ T/4 T/6T and the transmittance curve of $B_0 = 0$ T are shown in **Figure 4B**. We can perceive that the transmitted phase changes significantly when different magnetic flux density is applied to the graphene metasurface and caused different phase shifts. Similar to the transmittance shifts, the maximum value of the phase shifts increases with the applied flux density, shown in **Figure 4C**.

Starting with an easy-to-understand physical phenomenon, we postulate that the carrier's motion in the two-dimensional graphene surface will be deflected under the vertical magnetostatic field applied. If graphene is patterned as a THz metasurface, its resonance properties are closely related to the oscillation direction of the carriers in the pattern. When a magnetostatic field is applied, the oscillation deflection of the carriers causes a significant change in the transmittance properties of the graphene metasurface. Therefore, the external magnetostatic field can be used to control the transmittance characteristics of graphene metasurface and could be used to realize a dynamically tunable THz graphene metasurface. The postulation is confirmed by a simply designed metasurface. Parameters such as resonance frequency, transmittance, and transmitted phase of the metasurface are numerically studied. It is shown that these parameters are obviously changed when different magnetostatic fields are applied, and the shifts of these parameters are increasing with the increase of the applied magnetostatic field. Therefore, this study demonstrates that

the magnetostatic field can be used as an effective magneto-controlled method for the design of dynamically tunable metasurfaces in the THz regime.

It should be noted that the conventional electrostatic-controlled method [39] mainly regulates the Fermi level of graphene through electrical bias to control the properties of graphene metasurface, while our magneto-controlled one regulates the oscillating current of the carriers to control the transmittance properties of graphene metasurface. There are essential differences between the two. Compared with the conventional method, one advantage of the magneto-controlled method is that when the magnetic bias is used for control, it is not necessary to connect all the graphene patterns, as this will severely limit the flexibility of metasurface design. Although the magneto-controlled mechanism also depends on adjusting the Fermi level of graphene to an appropriate value, it essentially adds a new degree of tunable freedom. The combination of the magneto-controlled method and other control methods may give new opportunities for dynamically controlled graphene metasurface.

Finally, since the main purpose of this work is to demonstrate our new method of dynamically controlling the transmittance characteristics of the patterned graphene metasurface using a magnetostatic field, our focus is on the analysis and numerical verification of its working principle. Therefore, we have designed an intuitive and simple cut-wire structure to facilitate our interpretation of the principle. In recent years, several important local field enhancement mechanisms in the field of electromagnetic metasurface research, such as bound states in the continuum (BIC) [40], anople [41, 42], and Fano [43, 44], may indicate the direction for further improvement of the efficiency of the magneto-controlled metasurface. The introduction of one or more of the above mechanisms into the magneto-controlled metasurface would increase the response sensitivity while reducing the value of excitation magnetic field intensity.

CONCLUSION

In conclusion, we proposed a magneto-controlled method to manipulate the transmittance properties of the incident THz wave. To confirm this idea, a graphene-based THz metasurface comprised of graphene cut-wire arrays was investigated for proof-of-principle demonstration. The introduced vertical electrostatic field deflects the carriers in graphene and changes the transmittance characteristics of the metasurface. By adjusting the value of the applied magnetic flux density, the transmittance characteristics related parameters can be dynamically controlled, and the dynamically tunable metasurface is realized. Our results provide a new dimension for the design of graphene-based dynamically tunable THz metasurfaces.

DATA AVAILABILITY STATEMENT

The raw data supporting the conclusions of this article will be made available by the authors, without undue reservation.

AUTHOR CONTRIBUTIONS

YL designed and simulated the structure. All authors analyzed and discussed the results. YL and YW wrote the manuscript. The project was conceived and supervised by YW.

FUNDING

REFERENCES

1. Williams GP. Filling the THz gap—high power sources and applications. *Rep Prog Phys* (2006) 69(2):301–26. doi:10.1088/0034-4885/69/2/R01

2. Cunningham PD, Valdes NN, Vallejo FA, Hayden LM, Polishak B, Zhou X-H, et al. Broadband terahertz characterization of the refractive index and absorption of some important polymeric and organic electro-optic materials. *J Appl Phys* (2011) 109(4):043505. doi:10.1063/1.3549120

3. Tonouchi M. Cutting-edge terahertz technology. *Nat Photon* (2007) 1(2): 97–105. doi:10.1038/nphoton.2007.3

4. Nagatsuma T, Ducournau G, Renaud CC. Advances in terahertz communications accelerated by photonics. *Nat Photon* (2016) 10(6):371–9. doi:10.1038/nphoton.2016.65

5. Saeedkia D. *Handbook of terahertz technology for imaging, sensing and communications*. Woodhead Publishing Limited (2013).

6. Withayachumnankul W, Yamada R, Fujita M, Nagatsuma T. All-dielectric rod antenna array for terahertz communications. *APL Photonics* (2018) 3(5): 051707. doi:10.1063/1.5023787

7. Tripathi SK, Kumar M, Kumar A. Graphene based tunable and wideband terahertz antenna for wireless network communication. *Wireless Network* (2019) 25(7):4371–81. doi:10.1007/s11276-019-02101-8

8. Zhao Q, Zhou J, Zhang F, Lippens D. Mie resonance-based dielectric metamaterials. *Mater Today* (2009) 12(12):60–9. doi:10.1016/S1369-7021(09) 70318-9

9. Smith DR, Padilla WJ, Vier DC, Nemat-Nasser SC, Schultz S. Composite medium with simultaneously negative permeability and permittivity. *Phys Rev Lett* (2000) 84(18):4184–7. doi:10.1103/PhysRevLett.84.4184

10. Shelby RA, Smith DR, Schultz S. Experimental verification of a negative index of refraction. *Science* (2001) 292(5514):77–9. doi:10.1126/science.1058847

11. Sihvola A. Metamaterials in electromagnetics. *Metamaterials* (2007) 1(1):2–11. doi:10.1016/j.metmat.2007.02.003

12. Pendry JB, Schurig D, Smith DR. Controlling electromagnetic fields. *Science* (2006) 312(5781):1780–2. doi:10.1126/science.1125907

13. Yu N, Capasso F. Flat optics with designer metasurfaces. *Nat Mater* (2014) 13(2):139–50. doi:10.1038/nmat3839

14. Fan KB, Suen JY, Liu X, Padilla WJ. All-dielectric metasurface absorbers for uncooled terahertz imaging. *Optica* (2017) 4(6):601–4. doi:10.1364/OPTICA.4.000601

15. Cole MA, Powell DA, Shadrivov I. Strong terahertz absorption in all-dielectric Huygens' metasurfaces. *Nanotechnology* (2016) 27(42):424003. doi:10.1088/0957-4484/27/42/424003

16. Wang J, Hao T, Wang Y, Li X, Liu J, Zhou Z. Liquid crystal terahertz modulator with plasmon-induced transparency metamaterial. *Optic Express* (2018) 26(5): 5769–76. doi:10.1364/OE.26.005769

17. Grebenchukov AN, Zaitsev AD, Novoselov MG, Kovalska EO, Baldycheva AV, Khodzitsky MK. Multi-layer graphene based tunable metasurface for terahertz wave control. In: Zhang C, Zhang XC, Tani M, editors. *Infrared, millimeter-wave, and terahertz technologies V* (2018).

18. Xing Q, Wang C, Huang S, Liu T, Xie Y, Song C, et al. Tunable graphene split-ring resonators. *Physical Review Applied* (2020) 13(4):041006. doi:10.1103/PhysRevApplied.13.041006

19. Schwierz F. Graphene transistors. *Nat Nanotechnol* (2010) 5(7):487–96. doi:10.1038/nnano.2010.89

20. Su W, Liu YC, Chen BY. Multiple Fano resonances in asymmetric rectangular ring resonator based on graphene nanoribbon. *Results in Physics* (2020) 17: 103121. doi:10.1016/j.rinp.2020.103121

21. Liu CX, Zha S, Liu P, Yang C, Zhou Q. Electrical manipulation of electromagnetically induced transparency for slow light purpose based on metal-graphene hybrid metamaterial. *Applied Sciences-Basel* (2018) 8(12): 2672. doi:10.3390/app8122672

22. Kim TT, Oh SS, Kim H-D, Park H-S, Hess O, Min B, et al. Electrical access to critical coupling of circularly polarized waves in graphene chiral metamaterials. *Sci Adv* (2017) 3(9):e1701377. doi:10.1126/sciadv.1701377

23. Dabidian N, Kholmanov IN, Khanikaev A, Tatar K, Trendafilov S, Mousavi SH, et al. Electrical switching of infrared light using graphene integration with plasmonic Fano resonant metasurfaces. *ACS Photonics* (2015) 2(2):216–27. doi:10.1021/ph5003279

24. Rathi S, Lee I, Lim D, Wang J, Ochiai Y, Aoki N, et al. Tunable electrical and optical characteristics in monolayer graphene and few-layer MoS2 heterostructure devices. *Nano Lett* (2015) 15(8):5017–24. doi:10.1021/acs.nanolett.5b01030

25. Balandin AA, Ghosh S, Bao W, Calizo I, Teweldebrhan D, Miao F, et al. Superior thermal conductivity of single-layer graphene. *Nano Lett* (2008) 8(3): 902–7. doi:10.1021/nl0731872

26. Weber P, Güttinger J, Noury A, Vergara-Cruz J, Bachtold A. Force sensitivity of multilayer graphene optomechanical devices. *Nat Commun* (2016) 7:12496. doi:10.1038/ncomms12496

27. Fan Y, Wei Z, Zhang Z, Li H. Enhancing infrared extinction and absorption in a monolayer graphene sheet by harvesting the electric dipolar mode of split ring resonators. *Opt Lett* (2013) 38(24):5410–3. doi:10.1364/OL.38.005410

28. Fan YC, Shen N-H, Koschny T, Soukoulis CM. Tunable terahertz meta-surface with graphene cut-wires. *ACS Photonics* (2015) 2(1):151–6. doi:10.1021/ph500366z

29. Wang XF, Liu G-D, Xia S-X, Haiyu M, Shang X, He P, et al. Dynamically tunable Fano resonance based on graphene metamaterials. *IEEE Photon Technol Lett* (2018) 30(24):2147–50. doi:10.1109/LPT.2018.2879540

30. Zhang J, Wei X, Rukhlenko ID, Chen H-T, Zhu W. Electrically tunable metasurface with independent frequency and amplitude modulations. *ACS Photonics* (2020) 7(1):265–71. doi:10.1021/acsphotonics.9b01532

31. Zhang J, Zhang H, Yang W, Chen K, Wei X, Feng Y, et al. Dynamic scattering steering with graphene-based coding metamirror. *Advanced Optical Materials.* (2020) 8:2000683. doi:10.1002/adom.202000683

32. Wen Y, Zhou J. Artificial nonlinearity generated from electromagnetic coupling metamolecule. *Phys Rev Lett* (2017) 118(16):167401. doi:10.1103/PhysRevLett.118.167401

33. Liu C, Bai Y, Zhou J, Zhao Q, Qiao L. A review of graphene plasmons and its combination with metasurface. *J Kor Chem Soc* (2017) 54(5):349–65.

34. Wen Y, Zhou J. Artificial generation of high harmonics via nonrelativistic thomson scattering in metamaterial. *Research* (2019) 2019:8959285. doi:10.34133/2019/8959285

35. Fang Z, Thongrattanasiri S, Schlather A, Liu Z, Ma L, Wang Y, et al. Gated tunability and hybridization of localized plasmons in nanostructured graphene. *ACS Nano* (2013) 7(3):2388–95. doi:10.1021/nn3055835

36. Yan HG, Low T, Zhu W, Wu YQ, Freitag M, Li XS, et al. Damping pathways of mid-infrared plasmons in graphene nanostructures. *Nat Photon* (2013) 7(5): 394–9. doi:10.1038/nphoton.2013.57

37. Pol BVD. Frequency modulation. *Proc Inst Radio Eng* (1930) 18(7):1194–205.

38. Li G, Wen-jun G, Yan jun Z, Yan-li L, Yu-long H, Yan-hu S, et al. Polarization-controlled optical switch based on surface plasmon. *Acta Photonica Sin* (2020) 49(3):326001. doi:10.3788/gzxb20204903.0326001

39. Vakil A, Engheta N. Transformation optics using graphene. *Science* (2011) 332(6035):1291–4. doi:10.1126/science.1202691

40. Hsu CW, Zhen B, Stone AD, Joannopoulos JD, Soljačić M. Bound states in the continuum. *Nature Reviews Materials* (2016) 1(9):16048. doi:10.1038/natrevmats.2016.48

41. Miroshnichenko AE, Evlyukhin AB, Yu YF, Bakker RM, Chipouline A, Kuznetsov AI, et al. Nonradiating anapole modes in dielectric nanoparticles. *Nat Commun* (2015) 6:8069. doi:10.1038/ncomms9069

42. Zhang TY, Che Y, Chen K, Xu J, Xu Y, Wen T, et al. Anapole mediated giant photothermal nonlinearity in nanostructured silicon. *Nat Commun* (2020) 11(1):3027. doi:10.1038/s41467-020-16845-x

43. Campione S, Guclu C, Ragan R, Capolino F. Enhanced magnetic and electric fields via Fano resonances in metasurfaces of circular clusters of plasmonic nanoparticles. *ACS Photonics* (2014) 1(3):254–60. doi:10.1021/ph4001313

44. Panaro S, De Angelis F, Toma A. Dark and bright mode hybridization: from electric to magnetic Fano resonances. *Optic Laser Eng* (2016) 76:64–9. doi:10.1016/j.optlaseng.2015.03.019